

Stochastic dynamics in a two-dimensional oscillator near a saddle-node bifurcation

M. E. Inchiosa,* V. In,† and A. R. Bulsara‡

Space and Naval Warfare Systems Center San Diego, Code D363, 49590 Lassing Road, San Diego, California 92152-6147

K. Wiesenfeld§

School of Physics, Georgia Institute of Technology, Atlanta, Georgia 30332

T. Heath||

Georgia Tech Research Institute, 7220 Richardson Rd., Smyrna, Georgia 30080

M. H. Choi¶

School of Physics, Georgia Institute of Technology, Atlanta, Georgia 30332

(Received 22 November 2000; published 22 May 2001)

We study the oscillator equations describing a particular class of nonlinear amplifier, exemplified in this work by a two-junction superconducting quantum interference device. This class of dynamic system is described by a potential energy function that can admit minima (corresponding to stable solutions of the dynamic equations), or “running states” wherein the system is biased so that the potential minima disappear and the solutions display spontaneous oscillations. Just beyond the onset of the spontaneous oscillations, the system is known to show significantly enhanced sensitivity to very weak magnetic signals. The global phase space structure allows us to apply a center manifold technique to approximate analytically the oscillatory behavior just past the (saddle-node) bifurcation and compute the oscillation period, which obeys standard scaling laws. In this regime, the dynamics can be represented by an “integrate-fire” model drawn from the computational neuroscience repertoire; in fact, we obtain an “interspike interval” probability density function and an associated power spectral density (computed via Renewal theory) that agree very well with the results obtained via numerical simulations. Notably, driving the system with one or more time sinusoids produces a noise-lowering injection locking effect and/or heterodyning.

DOI: 10.1103/PhysRevE.63.066114

PACS number(s): 05.45.-a, 05.40.Ca, 02.50.Ey, 02.30.Hq

I. INTRODUCTION

The response of nonlinear dynamic systems to small perturbations, applied when the system is poised at (or just past) the onset of a bifurcation, has elicited considerable interest in recent years. The added sensitivity in this regime close to a bifurcation can be exploited as a means of signal amplification [1,2] in a large class of nonlinear dynamic systems. Conversely, the increased sensitivity can amplify environmental fluctuations and degrade a system’s signal to noise ratio and its signal transducing performance [3,4]. Nonlinear dynamic systems can also display a variety of interference phenomena due to competing periodic effects. Possibly the most widely known phenomenon is the generation of “combination resonances” when two tones of frequencies ω_1 and ω_2 are “mixed” together in a nonlinear system. In this case, the output power spectral density (PSD) contains a response at the combinations $|m\omega_1 \pm n\omega_2|$ where m, n are positive integers (there are selection rules depending, for instance, on the symmetry of the potential energy function, that put addi-

tional constraints on m, n). These interference effects were studied as early as the turn of the twentieth century by von Helmholtz [5].

However, a large class of two-dimensional (2D) nonlinear systems, exemplified in this work by the two-junction or dc superconducting quantum interference device (SQUID), is known to display *spontaneous* (i.e., in the absence of external driving signals) oscillations when the dynamical system crosses a threshold through a bifurcation [6]. The oscillations are periodic but nonsinusoidal, approaching sinusoidal behavior as one goes farther past the bifurcation. The oscillation frequency is a function of the “distance” past the onset of the bifurcation, and displays a characteristic scaling behavior with respect to the bias parameter that controls the bifurcation [6]. Applying an external sinusoidal signal to the system in this state of spontaneous oscillation yields a frequency mixing (this has, in fact, been observed by us in the dc SQUID [7]) that is quite analogous to the combination resonance generation described above.

The above behavior becomes even richer and more complex in the presence of background noise. The stochastic resonance (SR) effect, only one of a large class of noise-mediated cooperative phenomena, has already received a lot of attention because of its potential capability to improve the sensitivity of the *nonlinear dynamic* system to weak deterministic signals [8]. Recently, the effect has been studied in dc SQUIDs [9] with the idea of exploiting the background noise to improve sensitivity, rather than trying to devise

*Electronic address: inchiosa@spawar.navy.mil

†Electronic address: visarath@spawar.navy.mil

‡Electronic address: bulsara@spawar.navy.mil

§Electronic address: kw2@prism.gatech.edu

||Electronic address: ted.heath@gtri.gatech.edu

¶Electronic address: Mee.Choi@physics.gatech.edu

ever-more-sophisticated shielding and noise-cancellation procedures. SQUIDs [10] are the most sensitive detectors of magnetic fields and, with enhanced noise-tolerance, are likely to find applications in fields as diverse as biomagnetics, geophysics, communications, and assorted remote sensing applications.

In this work, we consider a dc SQUID as a prototype 2D system that traverses a saddle-node bifurcation when a control or bias parameter crosses a critical value. In a recent paper, the spontaneous oscillation frequency of the solutions (in the so-called ‘‘running regime’’ past the critical point) was computed [11], and we reproduce the salient features of that calculation for completeness. We then explore the effects of locking the intrinsic oscillations to an external driving signal; the phenomenon of background noise-suppression via frequency locking (first observed in charge density wave experiments [12] and later quantified via a very simple theory involving a circle map representation of the locked dynamics [13]) is examined in some detail. As part of our description of the system behavior in the neighborhood of the critical point, an interesting analogy with simple (integrate-fire) models of neural firing is exposed. Finally, we study some heterodyning effects (nonlinear production of sum and difference frequencies) arising out of the introduction of a time-sinusoidal target signal (in addition to the locking signal).

The paper is organized as follows. In Sec. II we write down the dc SQUID equations of motion and normal form equations, and we study their oscillatory solutions in the absence of driving. In Sec. III we calculate the shifted oscillation frequency and synchronization boundaries for the case of periodic forcing, in the absence of noise. We analytically study the normal form augmented with noise in Sec. IV. The interesting phenomena of noise suppression through injection locking and heterodyning are studied in Sec. V using numerical simulations with deterministic and stochastic forcing. We discuss our conclusions in Sec. VI.

II. BACKGROUND

The dc SQUID is a superconducting loop interrupted by two symmetrically placed ‘‘weak links’’ (Josephson junctions). Its dynamics are described by equations for the Schrödinger phase differences δ_i across the (assumed identical) Josephson junctions [14,15]

$$\tau \dot{\delta}_i = \frac{I_b}{2} + (-1)^i I_s - I_0 \sin \delta_i + F_i(t), \quad i=1,2, \quad (1)$$

where I_s , the circulating current induced in the loop by an externally applied magnetic flux, can be written in the form $\beta(I_s/I_0) = \delta_1 - \delta_2 - 2\pi(\Phi_e/\Phi_0)$. Here, $\tau = \hbar/(2eR)$ is a characteristic time constant (R being the normal state resistance of the junctions), $\beta = 2\pi LI_0/\Phi_0$ is the nonlinearity parameter, L is the loop inductance, I_0 is the junction critical current, and $\Phi_0 \equiv h/(2e)$ is the flux quantum. The independent additive noise terms $F_i(t)$ account for thermal noise arising due to the junction resistances. These terms are taken to have zero mean and to be Gaussian and delta correlated:

$\langle F_i(t) \rangle = 0$, $\langle F_i(t) F_j(t') \rangle = \tilde{\sigma}^2 \delta_{ij} \delta(t-t')$. The two natural experimental control parameters are the applied dc magnetic flux Φ_e and the dc bias current I_b , which we take to be symmetrically applied to the loop.

It is convenient to introduce a scaled time, applied flux $\Phi_{ex} \equiv \Phi_e/\Phi_0$, bias current $J \equiv I_b/(2I_0)$, and noise strength $\sigma = \tilde{\sigma}/\sqrt{\tau}$, and to rewrite the differential equations in terms of the sum and difference variables [14,16] $\Sigma \equiv (\delta_1 + \delta_2)/2$, $\delta \equiv (\delta_1 - \delta_2)/2$. Dropping the noise terms for now, we obtain

$$\begin{aligned} \dot{\delta} &= -\frac{2}{\beta}(\delta - \pi\Phi_{ex}) - \cos \Sigma \sin \delta, \\ \dot{\Sigma} &= J - \cos \delta \sin \Sigma. \end{aligned} \quad (2)$$

For sufficiently small bias current magnitude $|J|$, the system is attracted to a stable fixed point ($\delta = \delta_0$, $\Sigma = \Sigma_0$), whose position is a function of the three system parameters β , Φ_{ex} , and J . For fixed Φ_{ex} and β , there is a critical bias current J_c above which the stable superconducting state is destroyed; for $J > J_c$, the phase variables (δ_1, δ_2) or (δ, Σ) display periodic oscillation. The threshold J_c can be computed [15], in good agreement with experiment. Just past the bifurcation point (i.e., for J just exceeding J_c), the system encounters a ‘‘bottleneck’’ once each period near the point where a stable (node) fixed point annihilated with an unstable (saddle) fixed point. The term ‘‘saddle-node connection’’ refers to the existence of orbits connecting each node to a saddle and each saddle to the ‘‘next’’ node. When the bifurcation occurs, a running state is created in a global bifurcation, with the chain of (merged) saddle-node-saddle connections giving rise to an attractor. Near the bifurcation, the ensuing oscillations have the form of relaxation oscillations [16].

The resulting oscillation frequency of the circulating current I_s is generally very high, so that usually only the time-averaged quantity \bar{I}_s is measured in experiments (see, however, Ref. [17], where the oscillations were actually observed and the frequency computed in the extreme limiting case of $\beta \ll 1$). Thus, the SQUID’s response to an applied flux Φ_{ex} can be described via an \bar{I}_s vs Φ_{ex} transfer characteristic, from which the input-output gain (i.e., transfer characteristic slope) or the output signal-to-noise ratio (SNR) at the frequency of a weak injected signal (and in the presence of a noise floor) may be calculated as a function of the bias parameters (J, Φ_{ex}) [9,15]. The optimal response (highest gain or output SNR) is obtained just beyond the bifurcation and the onset of oscillations.

A general analytical solution of the dynamics (2) is not available; however, we can derive an approximate normal form solution close to the bifurcation (see Ref. [11] for details). We assume the dc bias flux Φ_{ex} to be fixed at some nonzero value; for $0 < J - J_c \ll 1$, we may Taylor expand the dynamics (2) (augmented with the equation $\dot{J} = 0$), around the critical fixed point $(\delta_0, \Sigma_0, J_c)$: $\delta = \delta_0 + x$, $\Sigma = \Sigma_0 + y$, with $|x|$, $|y| \ll 1$, and $J - J_c = O(2)$. We eliminate δ and Σ in favor of x and y and then transform to a rotated coordinate system u, v :

$$\begin{pmatrix} u \\ v \end{pmatrix} = \mathbf{S} \begin{pmatrix} x \\ y \end{pmatrix}; \quad \mathbf{S} = \begin{pmatrix} \cos \theta & \sin \theta \\ -\sin \theta & \cos \theta \end{pmatrix}, \quad (3)$$

where $\theta = (1/2)\arctan(-\beta \sin \delta_0 \sin \Sigma_0)$.

It follows that $\dot{u} = \lambda u + O(2)$, where $\lambda = -2/\beta - 2 \cos \Sigma_0 \cos \delta_0$, which must be negative so that the system orbits are attracted to the subspace $u=0$ on the faster (order one) time scale λ^{-1} . Consequently, the attracting subspace is $u = O(2)$. The evolution of v on the center manifold is given by

$$\dot{v} = (J - J_c) \cos \theta + \alpha v^2 + O(3), \quad (4)$$

where (see Ref. [11] for calculational details) $\alpha = -\sin \theta (C - D \sin 2\theta) + \cos \theta (D - C \sin 2\theta)$, $C = \frac{1}{2} \sin \delta_0 \cos \Sigma_0$, and $D = \frac{1}{2} \cos \delta_0 \sin \Sigma_0$.

Ignoring terms of cubic order and higher, we may now integrate Eq. (4) analytically, realizing that the dynamics (for small $J - J_c$) is dominated by the passage through the ‘‘bottleneck’’ where \dot{v} is at its smallest. We obtain the solution

$$v(t) = \sqrt{\frac{A_{\text{NF}}}{\alpha}} \tan \frac{\omega_0 t}{2}, \quad (5)$$

with $A_{\text{NF}} \equiv (J - J_c) \cos \theta$ and $\omega_0 \equiv 2\sqrt{A_{\text{NF}}\alpha}$, corresponding to a spontaneous oscillation period of

$$T_0 = \frac{\pi}{\sqrt{A_{\text{NF}}\alpha}}. \quad (6)$$

The normal form (NF) (4) corresponds to a highly overdamped particle moving in a potential

$$U(v) = -A_{\text{NF}}v - \frac{\alpha}{3}v^3. \quad (7)$$

Equation (6) conforms to the period scaling law that accompanies bifurcations of this type [6]. Figure 1 compares Eq. (6) with numerical simulations of the full nonlinear dynamics given by Eq. (2). The simulations were run for a range of system parameters β and Φ_{ex} (owing to a parameter symmetry, the full range of Φ_{ex} is between 0 and 0.5; we also note that SQUIDs are often fabricated to have $\beta \approx 1$). In the figure, the solid line is computed from Eq. (6), and the data are plotted over three decades in the reduced parameter $J - J_c$. In a typical SQUID, the current $J - J_c = 0.001$ might correspond to $\sim 5 - 10$ nA, with the oscillation frequency being in the GHz regime [9,16]. The agreement is good over the full range shown; it is excellent for smaller values of β and Φ_{ex} . The agreement grows systematically worse for larger β and Φ_{ex} , since either one reduces the size of the ‘‘bottleneck’’ regime. Even in the latter cases, the agreement improves in the limit $J \rightarrow J_c$, i.e., close enough to the bifurcation point.

We reiterate that the oscillations are *not* sinusoidal near the critical point, but approach sinusoidal behavior deep in the running regime; when $\Phi_{\text{ex}} = 0.5$, the oscillations become

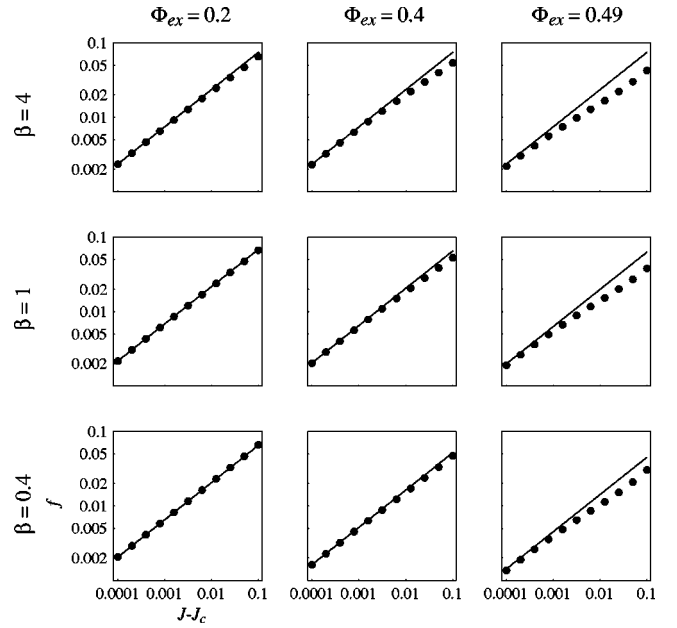


FIG. 1. Log-log plot of oscillation frequency f vs $J - J_c$ determined from direct numerical simulations (points) and the analytic prediction Eq. (6) (line), letting $f = 1/T_0$, for various values of β , Φ_{ex} , and J . Dimensionless units are used in all figures.

most closely sinusoidal, and the average circulating current vanishes. We note, also, that the dc bias flux Φ_{ex} could easily have been used as the control parameter (for constant bias current J) with an analogous scaling law for the spontaneous oscillations (this simply modifies the prefactor of Eq. (6), so T_0 scales with the same exponent in $\Phi_{\text{ex}} - \Phi_{\text{ex}1}$, $\Phi_{\text{ex}1}$ being the critical value of Φ_{ex} for a given fixed value of J). In fact, in laboratory settings and practical applications, the signal may be fed in either via the bias current or the applied flux, with engineering considerations (e.g., impedance matching constraints that depend strongly on the input frequency) often determining which method is preferred.

Note that the solution (5) is singular when the argument $\omega_0 t/2$ is an odd multiple of $\pi/2$. However, a better-behaved alternate NF [that agrees with Eq. (4) through $O(v^2)$] may be written down using the Taylor series expansion of $\cos v$ through $O(v^2)$:

$$\dot{v} = (J - J_c) \cos \theta + 2\alpha(1 - \cos v). \quad (8)$$

This has the solution

$$v(t) = 2 \arctan \left(\beta \tan \frac{\omega_{00} t}{2} \right), \quad (9)$$

where $\beta \equiv \sqrt{A_{\text{NF}}/(A_{\text{NF}} + 4\alpha)}$ and $\omega_{00} \equiv \sqrt{A_{\text{NF}}^2 + 4A_{\text{NF}}\alpha} = \omega_0 + O(2)$. The solution (9) is bounded and well behaved.

Figure 2 shows approximately two cycles of the circulating current time series derived from the full SQUID equation (dotted line) and normal form (8) (solid line) solutions. The agreement at this scale is excellent. In Fig. 3 we zoom in on one ‘‘spike’’ to reveal the difference between the solutions.

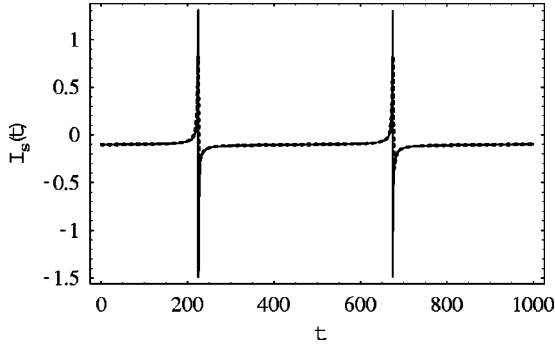


FIG. 2. Approximately two cycles of the full SQUID equation (dotted line) and normal form (solid line) circulating current time series solutions. $\beta=1.33$, $\Phi_{\text{ex}}=0.2$, and $J-J_c=0.0001$.

Simple averaging arguments can be applied to the normal form to yield the oscillation frequency when a driving signal is present. This is done in the following section.

III. PERIODIC FORCING AND INJECTION LOCKING

The use of normal forms is a powerful technique for the analysis of dynamical systems tuned near the onset of bifurcation [18]. Normal forms may be ‘‘augmented’’ with deterministic and/or stochastic driving terms in an attempt to extend the rigorous procedures to include these perturbing effects [19]. Intuitively, one expects this should work for sufficiently small perturbations, and indeed this approach has had notable successes, for example, in explaining the noise rise in Josephson parametric amplifiers [20] and the observed shifts in bifurcation points in a quasiperiodically driven magnetoresistive ribbon [2]. In at least one specific case the augmented normal form was derived explicitly, for period doubling in a bouncing ball system [4]. In general, the technique is used as a practical if nonrigorous modelling tool. In that spirit, we will consider deterministically augmented normal forms in this section, with stochastic driving terms to follow in the next section.

We begin with the modified normal form equation (8) describing the dynamics on the center manifold. We now include a periodic forcing in the bias current

$$J = J_c + A_c + q \sin(\omega t + \Theta), \quad (10)$$

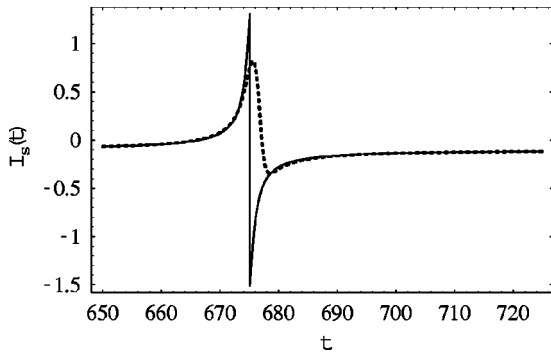


FIG. 3. Close-up view of one ‘‘spike’’ in the full SQUID equation (dotted line) and normal form (solid line) circulating current time series solutions. Same parameters values as Fig. 2.

where $A_c > 0$ and Θ are constants. With this bias current, the center manifold dynamics (8) becomes

$$\dot{v} = a - b \cos v + \varepsilon \sin(\omega t + \Theta), \quad (11)$$

where $a \equiv A_c \cos \theta + b$, $b \equiv 2\alpha$, and where, for notational convenience, the quantity $\varepsilon = q \cos \theta$ has been introduced. However, keep in mind that q is the amplitude of the ac component of the bias current.

A. Calculation of the shifted frequency

Our first step is to replace $v(t)$ in Eq. (11) by a ‘‘natural angle’’ ψ , i.e., an angle that, in the $\varepsilon=0$ limit, evolves at the constant rate ω_{00} [21]. By Eq. (9), we see that setting

$$\psi(t) = 2 \arctan\left(\frac{1}{\beta} \tan \frac{v(t)}{2}\right) \quad (12)$$

gives us an angle with the desired property: $\lim_{\varepsilon \rightarrow 0} \dot{\psi}(t) = \omega_{00}$. In terms of the natural angle $\psi(t)$, Eq. (11) becomes

$$\dot{\psi} = \omega_{00} + \left(\frac{\varepsilon}{\omega_{00}}\right) \sin(\omega t + \Theta) [a - b \cos \psi], \quad (13)$$

where, in terms of a and b , $\omega_{00} = \sqrt{a^2 - b^2}$.

As the driving amplitude ε is increased from zero, the SQUID’s running frequency will be pulled toward and eventually (for large enough ε) locked to the driving frequency. We now determine the SQUID’s shifted running frequency for a weak (i.e., below the locking threshold) driving signal. The phase difference between the SQUID and external oscillator will be defined as $\varphi \equiv \psi - (\omega t + \Theta)$. Therefore, from Eq. (13) we have

$$\dot{\varphi} = \omega_{00} - \omega + \left(\frac{\varepsilon}{\omega_{00}}\right) \sin(\omega t + \Theta) [a - b \cos(\varphi + \omega t + \Theta)]. \quad (14)$$

With a little trigonometry, this may be written as

$$\begin{aligned} \dot{\varphi} = \omega_{00} - \omega + \left(\frac{\varepsilon b}{2\omega_{00}}\right) \sin \varphi + \left(\frac{\varepsilon a}{\omega_{00}}\right) \\ \times \sin(\omega t + \Theta) - \left(\frac{\varepsilon b}{2\omega_{00}}\right) \sin(\varphi + 2\omega t + 2\Theta). \end{aligned} \quad (15)$$

Close to the locking threshold, φ evolves on a much slower time scale than that set by ω and ω_{00} . Therefore, we can time-average the right hand side of Eq. (15), taking φ to be effectively constant. Averaging Eq. (15) over one period of the driving signal leads to

$$\dot{\varphi} = \omega_{00} - \omega + \left(\frac{\varepsilon b}{2\omega_{00}}\right) \sin \varphi. \quad (16)$$

The solution of Eq. (16) is oscillatory, provided $\varphi(t)$ is interpreted modulo 2π . This frequency can be determined through separation of variables in Eq. (16), yielding

$$\omega_1 = \omega_{00} \sqrt{\Delta^2 - \left(\frac{\varepsilon b}{2\omega_{00}^2}\right)^2}, \quad (17)$$

where $\Delta \equiv (\omega - \omega_{00})/\omega_{00}$ is the normalized detuning. Recalling that $\varphi(t)$ is the phase difference between the SQUID oscillation phase and the external driving phase, the oscillation frequency of $[\varphi(t) \bmod 2\pi]$, ω_1 , equals the difference between the SQUID's shifted oscillation frequency ω_S and the external driving frequency ω . Taking proper account of signs for the two cases of positive and negative detuning, the SQUID's shifted frequency is given by

$$\omega_S = \omega - \text{sgn}(\Delta) \omega_1. \quad (18)$$

The two fundamental frequencies ω and ω_S will give rise to combination tones in the power spectrum of our nonlinear system's response at the frequencies

$$n_1 \omega \pm n_2 \omega_S, \quad (19)$$

where n_1, n_2 are integers. Figure 4 is a density plot showing the power spectra, computed via numerical simulation of the full (but noise-free) SQUID equations (2), for different driving amplitudes ε ; lighter shades indicate greater power. The "normalized amplitude" $q_N \equiv q/A_c = \varepsilon/[A_c \cos(\theta)]$ refers to the driving signal's amplitude, normalized by the amplitude A_c required to just reach the bifurcation point. The dotted lines superimposed on the density plot show the theoretically predicted locations of some of the lower order combination tones (19), revealing an elegant pattern. Notice how well the dotted lines track the locations of the actual peaks in the spectra.

B. Synchronization boundaries

Now we consider the case where the SQUID oscillator synchronizes with the external drive. Fixed-point solutions of Eq. (16) correspond to frequency locking between the SQUID and the external drive. Hence, we have

$$\omega - \omega_{00} = \left(\frac{\varepsilon b}{2\omega_{00}}\right) \sin \varphi. \quad (20)$$

Since $|\sin \varphi| \leq 1$, the frequency-locking boundaries are given by

$$\omega - \omega_{00} = \pm \left(\frac{\varepsilon_{\min} \alpha}{\omega_{00}}\right), \quad (21)$$

where ε_{\min} represents the minimum value of amplitude ε required for frequency locking. Solving for ε_{\min} reveals that it is proportional to the absolute value of the normalized detuning Δ :

$$\varepsilon_{\min} = \frac{\omega_{00}^2}{\alpha} |\Delta|. \quad (22)$$

Using $\varepsilon_{\min} = q_{\min} \cos \theta = q_{N,\min} A_c \cos \theta$ and $\omega_{00}^2 = 4A_c \alpha \cos \theta + (A_c \cos \theta)^2 \approx 4A_c \alpha \cos \theta$, we have

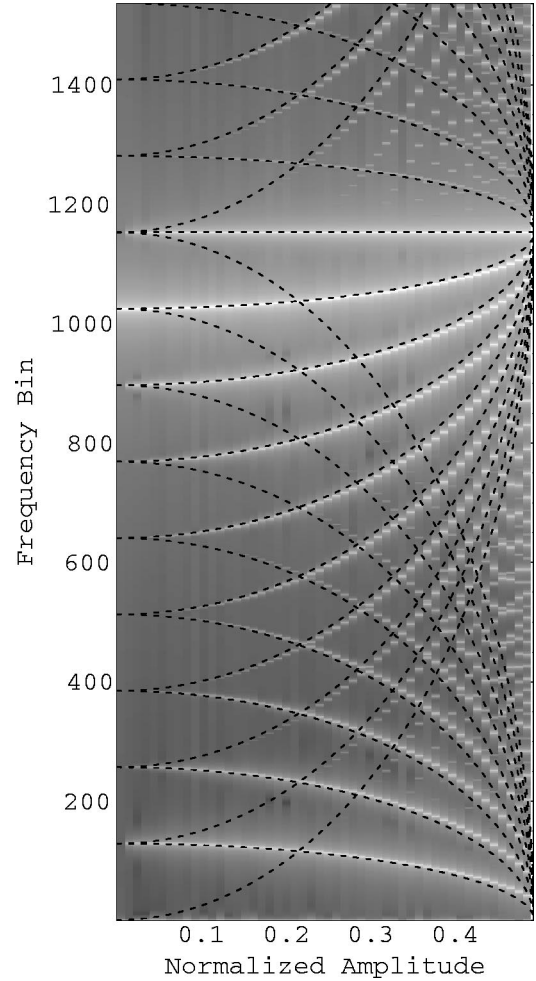


FIG. 4. Power spectra of SQUID response as a function of driving amplitude. Bin width is 6.01476×10^{-5} rad/sec. The driving amplitudes are below the level needed to induce frequency locking; rather, the SQUID oscillation frequency is "pulled" toward the driving frequency. The shaded "density plot" uses lighter shades to indicate higher power and was computed via numerical simulation. The dotted lines show the theoretical prediction (19) of the locations of fundamental and combination tone peaks in the power spectra. The SQUID's oscillation frequency in the absence of driving was $\omega_{00} = 0.06159$, corresponding to frequency bin 1024. The driving signal's frequency $\omega = 0.06929$ corresponds to bin $1024 + 128 = 1152$. $\beta = 1.33$, $\Phi_{\text{ex}} = 0.2$, $J = J_c + A_c + q \sin \omega t$, $J_c = 0.831258$, and $A_c = 0.002$.

$$q_{N,\min} = \frac{4A_c \alpha \cos \theta}{A_c \alpha \cos \theta} |\Delta| = 4|\Delta|. \quad (23)$$

This simple result tells us that, in order to lock the SQUID to the external drive, the ac bias current amplitude (normalized by A_c) must be at least 4 times the detuning. The accuracy of this prediction is very good, as can be judged from Fig. 8, where the theoretically predicted minimum locking amplitude (23) (bold line) and the same value as measured via numerical simulation of the full (but noise-free) SQUID equations (2) (dots) are compared.

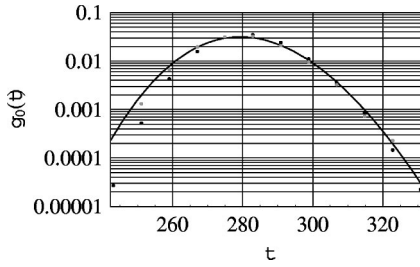


FIG. 5. First passage density functions obtained from the theoretical prediction (29) (solid line) and from simulations of the full SQUID equations (black dots) and the normal form equation (gray dots). $\beta=1.33$, $\Phi_{\text{ex}}=0.2$, $J=J_c+A_c$, $J_c=0.831258$, $A_c=0.000258$, $A_{\text{NF}}=0.000246232$, $\alpha=0.5105$, $\sigma^2=7.88697\times 10^{-8}$.

IV. LANGEVIN NOISE AND ITS EFFECT ON DYNAMICS NEAR THE CRITICAL POINT

We now consider augmenting the NF [Eq. (4) or (8)] with an additive noise term $F(t)$. For the time being, we assume that there is no external deterministic (time-sinusoidal) driving signal. The noise is taken to have zero mean and be Gaussian and delta correlated: $\langle F(t) \rangle = 0$, $\langle F(t)F(t') \rangle = \sigma^2 \delta(t-t')$. Very close to the critical point (corresponding to the onset of the saddle node bifurcation), we can assume that the dominant contribution to the oscillation period T_0 (6) arises from the low-slope, approximately linear portion of the potential (7). Therefore, to model this part of the motion we can try approximating the nonlinear potential (7) with a linear potential [as in the ‘‘perfect integrate-fire’’ (PIF) neuron model [22,23]]

$$U_1(v) = -A_{\text{PIF}}v, \quad (24)$$

where A_{PIF} is a bit larger than A_{NF} to improve the fit of the linear potential to the true cubic potential; later in this section we will show that $A_{\text{PIF}}=1.5A_{\text{NF}}$ provides excellent agreement between theoretical predictions derived using Eq. (24) and simulations of the full SQUID equations (see Figs. 5, 6).

Under the linear potential (24), the ‘‘velocity’’ variable satisfies

$$v(t) = v_0 + A_{\text{PIF}}t, \quad (25)$$

with v_0 being *preselected* so that the passage time to an absorbing barrier located at a_0 is exactly T_0 . This description is underpinned by the fact that the oscillations are spontaneous; in the presence of noise the mean period will be very

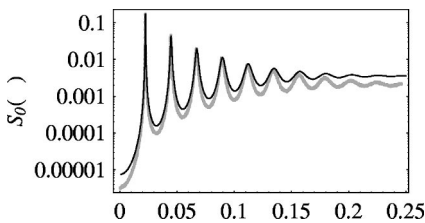


FIG. 6. Power spectral densities obtained from the theoretical prediction (30) (thin solid line) and from simulations of the full SQUID equations (gray points). Same parameters as Fig. 5.

close to the deterministic mean T_0 , and it will have some distribution with a variance and mode that depend on the noise intensity σ^2 . We readily obtain

$$v_0 = -\frac{A_{\text{PIF}}T_0}{2}, \quad a_0 = \frac{A_{\text{PIF}}T_0}{2}, \quad (26)$$

and the model has now been mapped onto the PIF neuron model. We assume that after every excursion to the absorbing barrier the state point is reset to the initial value v_0 , corresponding to a reinjection. Effectively, we have replaced the dynamics (4) by the PIF model

$$\dot{v} = A_{\text{PIF}} + F(t). \quad (27)$$

The mean ‘‘firing period’’ is T_0 (6), which incorporates the NF parameter α .

The approximation (27) should be very good near the critical point. If one draws a vertical line through v_0 to intersect the potentials $U(v)$, $U_1(v)$, then the separation of the potentials should be extremely small, i.e., $|U(v_0) - U_1(v_0)| \ll 1$. This leads to the requirement $|\alpha v_0^3/3| \ll 1$, and, substituting for v_0 , we have the condition

$$\frac{A_{\text{PIF}}^3}{\alpha} \ll 1, \quad (28)$$

which is well satisfied near the onset of the bifurcation and, in fact wherever one obtains good agreement between the exact and calculated oscillation periods as depicted in Fig. 1. Hence, the PIF description can be invoked in the running regime where our calculations of Sec. II are valid.

For the system (27) with the absorbing boundary condition, the first passage density function is given by [22,23]

$$g_0(t) = \frac{\Delta U_0}{\sqrt{2\pi\sigma^2 t^3}} \exp^{-(\Delta U_0 - A_{\text{PIF}}t)^2/2\sigma^2 t}, \quad (29)$$

where we introduce a ‘‘barrier height’’ $\Delta U_0 \equiv |a_0 - v_0| = A_{\text{PIF}}T_0$. It is very instructive that only this barrier height enters into all expressions; a knowledge of the initial point v_0 and the barrier location a_0 is not necessary. Equation (29), with $A_{\text{PIF}}=1.5A_{\text{NF}}$, gives a very good prediction of the first passage density function measured in simulations of the full SQUID equations and the normal form. Figure 5 shows excellent agreement for return times greater than or equal to the most probable time (the time at the mode of the distribution). These relatively long times emphasize the universal behavior that the models have in common. The disagreement at shorter times reflects the differences in the detailed behavior in the models close to a ‘‘spike.’’

The good agreement seen in Fig. 5 occurs also for lower noise levels. For higher noise levels, the noise begins to dominate the other terms in the differential equation(s), qualitatively changing the dynamics and rendering the previous analysis invalid.

Note that the mode t_m of the density function (29) is a function of noise [23], in contrast to the mean value which, to a high degree of accuracy, is simply the deterministic

crossing time T_0 (provided the noise is not too large). We reiterate that all our calculations are carried out in the oscillatory regime ($J > J_c$ for fixed Φ_e). On the other side of the critical point ($J < J_c$), we encounter ‘‘excitable’’ dynamics that can, close to the critical point, be represented by a particle in a near-parabolic potential. This approach, which is closely analogous to a ‘‘leaky integrate-fire’’ neuron model (or, simply, a noise-driven Ornstein-Uhlenbeck process with an absorbing barrier) [24], has recently been quantified [25].

From the first passage density function, $g_0(t)$, one may compute the output power spectral density (PSD), treating the ‘‘firing’’ process as being renewal (true to a high degree of approximation in the absence of periodic forcing) and using the Lukes formula [23,26] (disregarding any dc term):

$$S_0(\Omega) = \frac{|F_0(\Omega)|^2}{T_0} \operatorname{Re} \left[\frac{1 + \phi_0(\Omega)}{1 - \phi_0(\Omega)} \right], \quad (30)$$

where $\phi_0(\Omega) \equiv \int_0^\infty g_0(t) e^{i\Omega t} dt = \exp[\Delta U_0 (A_{\text{PIF}} - \sqrt{A_{\text{PIF}}^2 - 2i\sigma^2\Omega}) / \sigma^2]$ is the characteristic function of $g_0(t)$ and $F_0(\Omega)$ is the Fourier transform of a single pulse or ‘‘spike.’’ Although this approach is strictly true for a process consisting of identical pulses separated by random quiescent intervals, in the case of low noise the pulses in our system are relatively alike and the interpulse interval is nearly quiescent. Also, we do not have an analytical expression for the pulse shape or its Fourier transform. However, our very narrow pulses in the time domain correspond to very broad peaks in the frequency domain centered around zero frequency. Therefore, we can take $F_0(\Omega)$ to be approximately constant for $0 \ll \Omega \ll 1/(\text{pulse width})$. It should be clear that moving away from the bifurcation and deep into the running regime would result in less spiky, more rounded waveforms and therefore worsen the quality of this approximation.

Figure 6 shows good agreement between the theoretical prediction (30) of the PSD and simulations of the full SQUID equations when a constant value is chosen for $F_0(\Omega)$ such that we get a good fit to the height of the lowest frequency peaks. Simulations of the normal form equation yield similarly good agreement (not shown). Note that taking $F_0(\Omega)$ to be constant does cause the theoretical prediction to exceed the simulation result at high frequencies. In fact, when we numerically evaluate $F_0(\Omega)$ using a typical pulse generated in the simulations and then use this $F_0(\Omega)$ in Eq. (30), we do see better agreement (the correction is a factor of about 0.7 at $\Omega = 0.25$).

It is worth pointing out that the PSD given above contains some very interesting features due to the presence of the intrinsic oscillation frequency in the dynamics. These features have been discussed in Ref. [23], and we do not reproduce them here.

We now insert a time-sinusoidal signal. Then the noise-augmented NF reads

$$\dot{v} = A_c \cos \theta + \alpha v^2 + \varepsilon \sin \omega t + F(t), \quad (31)$$

where we will take $\varepsilon \ll A_c \cos \theta$, and ω as the smallest frequency in the system. Note, however that this ‘‘adiabatic’’

condition can be somewhat relaxed in practice (as in conventional stochastic resonance calculations [8], for example).

We must now set the initial condition v_{0s} and the absorbing barrier a_{0s} for the problem with the signal present. As before, we assume the important motion to occur through the bottleneck, ignoring the steep part of the potential. Then the relevant part of the ODE (31) can be integrated to give

$$v(t) = C + A_{\text{PIF}} t - \frac{\varepsilon}{\omega} \cos \omega t, \quad (32)$$

C being an integration constant. Setting $v = v_{0s}$ at time $t = 0$ determines C . Then we set $v = a_{0s}$ at time $t = T_s$, the period of the oscillations with signal present. Again, we can find for the ‘‘barrier height’’

$$a_{0s} - v_{0s} \equiv \Delta U_s = A_{\text{PIF}} T_s + \frac{\varepsilon}{\omega} (1 - \cos \omega T_s). \quad (33)$$

Note that $\Delta U_s(\varepsilon = 0) = \Delta U_0$, as it should.

We are now faced with the PIF model with a driving signal. As described in Ref. [23], we can derive the escape density $g(t)$:

$$g(t) = \frac{\Delta U_s}{\sqrt{2\pi\sigma^2 t^3}} \exp[-Z_-^2(t)] + H(t) \varepsilon (t \sin \omega t + \omega^{-1} \cos \omega t) \Phi_c(Z_+(t)) \times \exp \left[2tH(t) \left(A_{\text{PIF}} t - \frac{\varepsilon}{\omega} \cos \omega t \right) \right], \quad (34)$$

where we define

$$Z_\pm(t) \equiv \frac{\Delta U_s \pm [A_{\text{PIF}} t - (\varepsilon/\omega) \cos \omega t]}{\sqrt{2\sigma^2 t}}, \quad H(t) \equiv \frac{\Delta U_s}{\sigma^2 t^2},$$

and Φ_c is the complementary error function.

Equation (34) has been derived under some very stringent assumptions [23,24]. These include having a signal amplitude that is small compared to the drift (constant) term in Eq. (31), and the adiabatic assumption of low signal frequency. Accordingly, the applicability of Eq. (34) is severely restricted in many practical scenarios; however, one can relax the above constraints somewhat and still get the correct qualitative behavior [23,24].

To compute the PSD we might again consider using the Lukes formula (30) applied to the ‘‘spike’’ sequence, with T_0 replaced by T_s and $g(t)$ in place of $g_0(t)$. However, since the signal phase is not reset each time we cross the absorbing barrier and have reinjection, this can lead to some serious issues that revolve around the assumption of renewal behavior in using the Lukes formula. Not employing a phase reset following every ‘‘spike’’ means that successive spikes could be correlated, so that the Lukes formula is not strictly applicable. Resetting the phase of the signal following every ‘‘spike’’ ensures the process being renewal; however, this is an unreasonable approximation, except in very specific

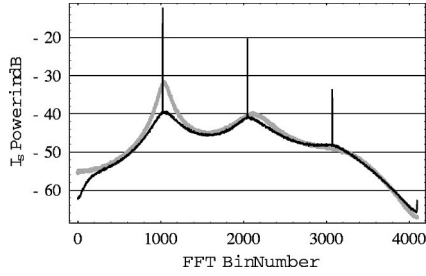


FIG. 7. Power spectrum of SQUID circulating current. Driving signal amplitude is $q=0$ (gray curve) and $q=0.0014$ (black curve). $\beta=2$, $\Phi_{\text{ex}}=0.495$, $J=J_c+A_c+q \sin \omega t$, $J_c=0.40731$, $A_c=0.002$, and $\omega=0.0479225$. There are two Gaussian noise sources of strength $\sigma^2=6.3096 \times 10^{-5}$ modeling thermal noise coming from the two Josephson junctions in the dc SQUID. Bin width is 4.67993×10^{-5} rad/sec.

cases. In any case, one would expect Eq. (30) to yield poorer agreement with increasing signal amplitude ϵ for the reasons stated earlier.

Note that in the absence of a phase reset following every ‘spike,’ we should introduce a random phase component ϕ and then average $g(t)$ with respect to ϕ 's density function $W(\phi)$:

$$\bar{g}(t) = \int_0^{2\pi} g(t, \phi) W(\phi) d\phi. \quad (35)$$

One can carry out the averaging in a variety of ways. One procedure is to use a variant of the distribution already derived by Zhou *et al.* [27]:

$$W(\phi) = \frac{1}{2\pi I_0(\epsilon \Delta U_s / \sigma^2)} \exp\left[\frac{\epsilon \Delta U_s}{\sigma^2} \cos \phi\right]. \quad (36)$$

For the weak signal case $\tilde{\epsilon} \equiv \epsilon/A_{\text{PIF}} \ll 1$ (for which this treatment is strictly valid), we can systematically expand Eq. (34) to $O(\tilde{\epsilon})$. When we insert the phase factors ϕ into the arguments of all the trigonometric functions, multiply by the distribution (36) and expand to $O(\tilde{\epsilon})$, we do not get any contribution (to this order only) from $W(\phi)$. Other authors [28] have suggested improvements on the phase-averaging procedure.

Given the vicissitudes and caveats associated with the introduction of time-inhomogenous terms into the leaky integrate-fire model and the fact that we will ultimately be concerned with more than one external signal, we do not further utilize the integrate-fire analogy for the case where driving signal(s) are present.

V. NUMERICAL SIMULATIONS WITH DETERMINISTIC AND STOCHASTIC FORCING

A. Low frequency noise suppression

Applying sinusoidal driving at or near the running frequency can produce an injection locking effect that tends to suppress the noise background in the neighborhood of the running frequency as well as near dc. Figure 7 illustrates the

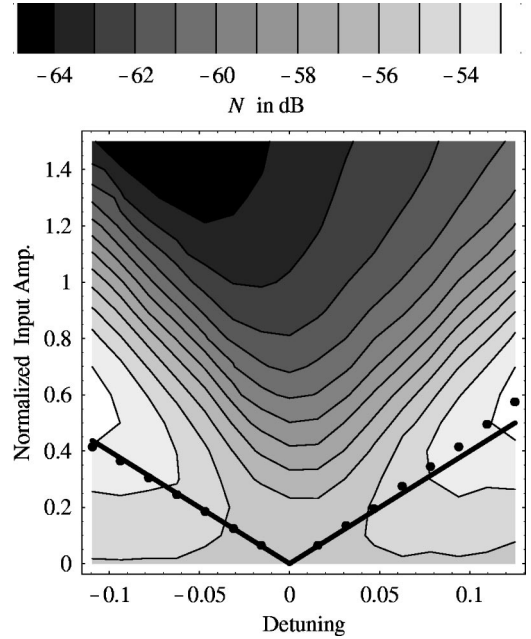


FIG. 8. Low frequency (3.125% of the running frequency) noise power as a function of input amplitude and detuning. An injection signal amplitude of $q=A_c=0.002$ just reaches the bifurcation point; ‘normalized input amplitude’ q_N is measured relative to this value. The detuning Δ equals the injection signal frequency ω minus the running state frequency of 0.0479225 rad/sec, measured relative to the running frequency. The bold line marks the theoretically predicted minimum amplitude required for locking in the absence of noise, while the dots mark the same quantity as measured via numerical simulation (again, in the absence of noise). Other parameter values as in Fig. 7

effect using a driving signal of amplitude $q=0.0014$ and frequency equal to the running frequency. At higher driving amplitudes, noise lowering occurs across the spectrum from dc to several times the running frequency. Similar effects appear to have been observed first in charge density wave experiments [12] and later were explained theoretically by a generic iterative map underlying the locking of the internal oscillation frequency to an external time-periodic signal [13].

Figure 8 shows the low frequency (about 3% of the running frequency) noise power as a function of input amplitude and detuning. Recall from Sec. III B that the bold line and dots mark the minimum amplitude required for locking in the absence of noise, as theoretically predicted Eq. (23) and as measured via numerical simulation, respectively. As a function of input amplitude, the low frequency noise power *rises* until the input amplitude reaches roughly the amplitude necessary to cause frequency locking. Increasing the input amplitude above this value then begins to cause a decrease in low frequency noise power. Eventually the noise power is suppressed significantly (up to approximately 10 dB) below its value in the absence of an injection locking driving signal.

B. Heterodyning

We have seen that injection locking can significantly suppress low frequency noise. What is its effect on low frequency sinusoidal signals? In the left panel of Fig. 9 we

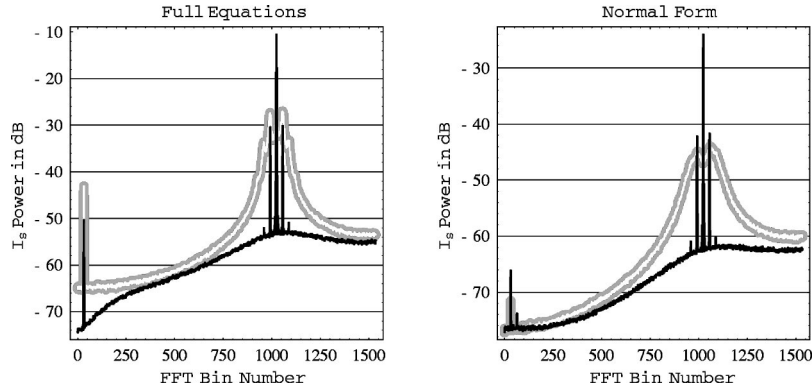


FIG. 9. Power spectrum of SQUID circulating current, derived from full SQUID equations (left panel) and normal form (right panel). Injection locking amplitude is $q=0$ (white curve with gray border) and $q=0.002$ (black curve). The target signal amplitude is $A_T = 0.00025$. Target signal frequency $\omega_T = .03125\omega$, and ω is set equal to the running frequency. $\beta=2$, $\Phi_{ex}=0.495$, $J=J_c + A_c + q \sin \omega t + A_T \sin \omega_T t$, $J_c=0.40731$, and $A_c=0.002$. For the full SQUID equations there are two Gaussian noise sources of strength $\sigma^2=6.3096 \times 10^{-6}$ each (one noise source for each of the two coupled equations in two variables), the power spectrum bin width is 4.67993×10^{-5} rad/sec, and $\omega=0.0479225$ (i.e., bin 1024). For the augmented normal form case there is just one Gaussian noise source of strength $\sigma^2=6.3096 \times 10^{-6}$, the power spectrum bin width is 6.2067×10^{-5} rad/sec, and $\omega=0.0635566$ (i.e., bin 1024).

illustrate the power spectrum of a SQUID driven by a low frequency sine wave in the absence and presence of a much higher frequency injection locking signal. Although injection locking reduces the low frequency noise, it also suppresses the low frequency signal. However, a strong heterodyning effect also occurs, resulting in the appearance of sidebands around the injection locking signal. The presence of a low frequency signal can be inferred from these sidebands, and in practice it may be more convenient to detect the low frequency signal at the higher frequency of these sidebands.

In the normal form case (right panel of Fig. 9), we do not see any low frequency noise suppression. However, we see a very interesting effect concerning detection of the low frequency target signal. Adding the injection locking signal appears to boost the low frequency signal considerably. Furthermore, the sidebands produced have a much greater signal strength and signal to noise ratio than the low frequency target signal itself. This suggests that it may be much more reliable to detect such a low frequency target signal via the high frequency sidebands in systems that are very accurately described by the normal form.

Note that Fig. 9 is meant to illustrate the *qualitative* similarities and differences between the full SQUID equations and the normal form. Recall that the normal form was ‘‘aug-

mented’’ with a noise term; however, this term was not rigorously derived from the SQUID equations. For comparison purposes, we have simply chosen to add the same strength noise term to the normal form equation as in each of the two SQUID equations. This choice is supported by the fact that it did give excellent agreement in the case of the first passage density function (Fig. 5)

Strong heterodyning effects are also seen for a high frequency target signal (at about 97% of the running frequency) in the presence of an injection locking signal at the running frequency (Fig. 10). This heterodyning effect might prove useful when the target signal frequency is quite high and it would be more convenient to filter, process, and detect it at a lower frequency.

VI. DISCUSSION

We were led to study the dc SQUID due to its wide applicability for magnetic sensing applications [10]. Earlier experimental and theoretical work has established that the best response to weak magnetic signals (in the presence of a background noise floor) is found just past the critical point. The goal of the present work has been to develop a reasonably broad understanding of the system dynamics in this re-

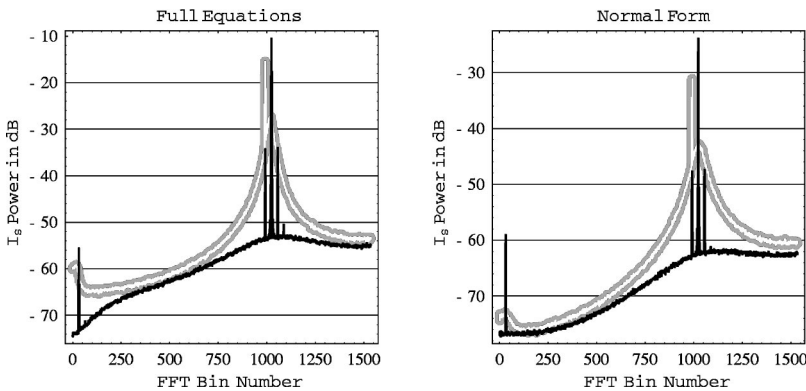


FIG. 10. Power spectrum of SQUID circulating current, derived from full SQUID equations (left panel) and normal form (right panel). Injection locking amplitude is $q=0$ (white curve with gray border) and $q=0.002$ (black curve). The target signal amplitude is $A_T=0.00025$. Target signal frequency $\omega_T=0.96875\omega$, and ω is set equal to the running frequency. Other parameters values as in Fig. 9.

gime, including the effects of periodic and stochastic perturbations.

The tool we found useful was normal form analysis. The normal form was modified in two ways, first by choosing a local form which simultaneously accommodated the global phase space topology, and second by adding forcing terms to model periodic and random perturbations. While these steps fall outside the rigorous treatment of center manifold mathematics, they have been successful in the past. Here again this approach does an excellent job, judging from comparisons against numerical simulations of the full system.

In this way, we have made a good deal of quantitative progress, deriving expressions near the bifurcation for the following: the spontaneous oscillation frequency and the spiky wave form in the absence of periodic or noisy perturbations, the frequency shift and onset of frequency locking in the presence of a weak periodic forcing, and the first passage density function and power spectral density in the presence of noise.

Under the combined influences of noise and periodic forcing, we have only qualitative progress, which is nonetheless suggestive. We find a suppression of low frequency noise due to injection locking. If a second (weak) periodic signal is present, a strong heterodyne effect occurs, leading to surprisingly clean high-frequency sidebands of the first (injection) drive. This leads to an intriguing alternative approach for detecting either very weak low- or very high-frequency signals for which dc SQUIDS may be particularly well suited. Curiously, while the augmented normal form does not show the noise suppression, it captures the heterodyning effects quite nicely.

ACKNOWLEDGMENTS

A.R.B., M.E.I., and V.I. acknowledge support from the Office of Naval Research (Physics Division). K.W. acknowledges summer support at SPAWAR through ONR/ASEE and support from ONR Grant No. N00014-99-1-0592.

-
- [1] M. J. Feldman, P. T. Parrish, and R. Y. Chiao, *J. Appl. Phys.* **46**, 4031 (1975).
 - [2] S. T. Vohra, L. Fabiny, and K. Wiesenfeld, *Phys. Rev. Lett.* **72**, 1333 (1994); S. T. Vohra and K. Wiesenfeld, *Physica D* **86**, 27 (1995).
 - [3] See, e.g., P. H. Bryant, R. Movshovich, and B. Yurke, *Phys. Rev. Lett.* **66**, 2641 (1991); B. Derighetti, M. Ravani, R. Stoop, P. Meier, P. Brun, and R. Badii, *ibid.* **55**, 1746 (1985); G. Ahlers, M. C. Cross, P. C. Hohenberg, and S. Safran, *J. Fluid Mech.* **110**, 297 (1981).
 - [4] K. Wiesenfeld and N. F. Tufillaro, *Physica D* **26**, 321 (1987).
 - [5] See, e.g., J. W. S. Rayleigh, *The Theory of Sound* (Dover, New York, 1945), Chap. 23, Vol. 2.
 - [6] See, e.g., S. Strogatz, *Nonlinear Dynamics and Chaos* (Perseus Press, New York, 1994).
 - [7] A. Bulsara, K. Wiesenfeld, and M. Inchiosa, *Ann. Phys. (Leipzig)* **9**, 655 (2000).
 - [8] For overviews see K. Wiesenfeld and F. Moss, *Nature (London)* **373**, 33 (1995); A. Bulsara and L. Gammitoni, *Phys. Today* **49** (3), 39 (1996); L. Gammitoni, P. Hänggi, P. Jung, and F. Marchesoni, *Rev. Mod. Phys.* **70**, 1 (1998).
 - [9] A. Hibbs, in *Applied Nonlinear Dynamics and Stochastic Systems Near the Millenium*, AIP Conf. Proc. 411, edited by J. Kadtko and A. Bulsara (AIP, New York, 1997); A. Hibbs and B. Whitecotton, *Appl. Supercond.* **6**, 495 (1999); M. Inchiosa, A. Bulsara, A. Hibbs, and B. Whitecotton, *Phys. Rev. Lett.* **80**, 1381 (1998).
 - [10] For a good overview see, e.g., J. Clarke, in *The New Superconducting Electronics*, edited by H. Weinstock and R. Ralston (Kluwer, Amsterdam, 1993).
 - [11] K. Wiesenfeld, A. Bulsara, and M. Inchiosa, *Phys. Rev. B* **62**, R9232 (2000).
 - [12] M. Sherwin and A. Zettl, *Phys. Rev. B* **32**, 5536 (1985).
 - [13] K. Wiesenfeld and I. Satija, *Phys. Rev. B* **36**, 2483 (1987).
 - [14] A. Barone and G. Paterno, *Physics and Applications of the Josephson Effect* (Wiley, New York, 1982). K. Likharev, *Dynamics of Josephson Junctions and Circuits* (Gordon and Breach, Philadelphia, 1984).
 - [15] M. Inchiosa, A. Bulsara, K. Wiesenfeld, and L. Gammitoni, *Phys. Lett. A* **252**, 20 (1999); M. Inchiosa and A. Bulsara, in *Stochastic and Chaotic Dynamics in the Lakes*, edited by D. S. Broomhead, E. Luchinskaya, P. V. E. McClintock, and T. Mullin (AIP, Melville, 2000), pp. 583.
 - [16] See, e.g., H. Koch in *Sensors, A Comprehensive Survey*, edited by W. Gopel, J. Hesse, and J. Zemel (VCH Publishers, New York, 1989), Vol. 5.
 - [17] K. Nakajima *et al.*, *J. Appl. Phys.* **60**, 3786 (1986).
 - [18] J. D. Crawford, *Rev. Mod. Phys.* **63**, 991 (1991).
 - [19] P. Bryant and K. Wiesenfeld, *Phys. Rev. A* **33**, 2525 (1986); P. Bryant, B. McNamara, and K. Wiesenfeld, *J. Appl. Phys.* **62**, 2898 (1987).
 - [20] P. Bryant, K. Wiesenfeld, and B. McNamara, *Phys. Rev. B* **36**, 752 (1987); P. Bryant, R. Movshovich, and B. Yurke, *Phys. Rev. Lett.* **66**, 2641 (1991).
 - [21] J. W. Swift, S. H. Strogatz, and K. Wiesenfeld, *Physica D* **55**, 239 (1992).
 - [22] G. Gerstein and B. Mandelbrot, *Biophys. J.* **4**, 41 (1964); C. Stevens, *ibid.* **4**, 417 (1964).
 - [23] A. Bulsara, S. Lowen, and D. Rees, *Phys. Rev. E* **49**, 4989 (1994).
 - [24] A. Bulsara, T. Elston, C. Doering, K. Lindenberg, and S. Lowen, *Phys. Rev. E* **53**, 3958 (1996).
 - [25] M. Eguia and G. Mindlin, *Phys. Rev. E* **61**, 6490 (2000).
 - [26] T. Lukes, *Proc. Phys. Soc. London* **78**, 153 (1961); S. Lowen and M. Teich, *Phys. Rev. E* **47**, 992 (1993).
 - [27] T. Zhou, F. Moss, and P. Jung, *Phys. Rev. A* **42**, 3161 (1990).
 - [28] M. Choi, R. Fox, and P. Jung, *Phys. Rev. E* **57**, 6335 (1998); H. Plesser and T. Geisel, *Phys. Rev. E* **59**, 7008 (1999).